catalysts

MDPI

Article

Partial Hydrogenation of Anthracene with In Situ Hydrogen Produced from Water-Gas Shift Reaction over Fe-Based Catalysts

He Liu *, Shiguang Fan, Xu Gong, Jian Wang, Aijun Guo, Kun Chen and Zongxian Wang

State Key Laboratory of Heavy Oil Processing, College of Chemical Engineering, China University of Petroleum (East China), 66 Changjiang West Road, Qingdao Economic Development Zone, Qingdao 266580, China; sgf@s.upc.edu.cn (S.F.); gongxu@boe.com.cn (X.G.); j.wang@s.upc.edu.cn (J.W.); ajguo@upc.edu.cn (A.G.); chenkun@upc.edu.cn (K.C.); zxwang@upc.edu.cn (Z.W.)

* Correspondence: liuhe@upc.edu.cn; Tel.: +86-15588671352

Received: 31 October 2020; Accepted: 23 November 2020; Published: 25 November 2020

Abstract: Partial hydrogenation of anthracene under CO-H_2O, N_2-H_2O, and H_2-H_2O over Fe-based catalysts was studied at 400 °C and 10 MPa. Results show that the Fe-based catalysts display obvious catalytic activity for anthracene hydrogenation under CO-H_2O instead of hydrogenation under N_2-H_2O and H_2-H_2O. The activity follows in the order of $Fe(NO_3)_3{\cdot}9H_2O$ > Fe naphthenate > $FeSO_4{\cdot}7H_2O$. Even though the amount of molecular hydrogen remains higher than that of in situ hydrogen, the anthracene conversion with in situ hydrogen is remarkably higher. It demonstrates that the in situ hydrogen is more active than molecular hydrogen for PAH hydrogenation. To further reveal the exact fate of these Fe-based catalysts, the decomposed products under CO-H_2O, N_2-H_2O and H_2-H_2O were characterized by TG, XRD, and TEM. Results indicate that the Fe_3O_4 species play a key role in hydrogenation of anthracene under CO and H_2O. Higher catalytic activity for $Fe(NO_3)_3{\cdot}9H_2O$ is due to its complete decomposition at 350 °C to acquire higher concentration of active Fe_3O_4 species. The possible form of in situ hydrogen during this process is also discussed. Given that heavy oil contains abundant polyaromatics, these results are meaningful for enhancing hydrogen shuttling to heavy oil by producing natural hydrogen donors and, thus, benefiting the high-efficient upgrading.

Keywords: PAH hydrogenation; in situ hydrogen; water gas shift reaction; natural hydrogen donors

1. Introduction

Heavy oil is characterized by high viscosity and low mobility, which poses great difficulties and detrimental hazards to its transportation [1]. In situ partial upgrading of heavy oil to obtain synthetic oil that meets the specification of transportation (mainly viscosity, American Petroleum Institute relative density (°API), and stability) has attracted much attention as the global petroleum supply is becoming much inferior [2]. The condensation of large radicals from pyrolysis of heavy oil molecules to induce coke formation significantly restricts the promotion of upgrading efficiency and deteriorates the stability of synthetic oil [3–5]. Active hydrogen could promptly scavenge the large cracked heavy oil radicals and effectively inhibit the coke formation progress [6]. However, the high cost of molecular hydrogen obstructs its utilization to a large extent. To explore the alternative active hydrogen sources remains a great concern for more efficient heavy oil thermal upgrading.

The in situ hydrogen produced from the water-gas shift reaction (WGSR) is recognized as an important hydrogen source and has been initially applied in the field of coal liquefaction [7]. Based on this type of hydrogen, Ng et al. developed a novel single-stage emulsion upgrading process for heavy

oil, in which the water separation and the dilution are both avoided [8–10]. It was reported that the viscosity reduction and API gravity improvement for heavy oil partial upgrading over in situ hydrogen was even more excellent than that over molecular hydrogen in the presence of dispersed MoS_2 catalysts [11]. But this process is still partly confined by the requirement of costly catalysts. In our previous work [12], it was observed that the coke induction for partial upgrading of heavy residue from Canadian oil sand bitumen could be postponed by the in situ hydrogen in the absence of catalysts. Nevertheless, the coke inhibition capability was shown to be lower than molecular hydrogen. The inconsistency can be attributed to the different hydrogenation behaviors of complex species in heavy oil. Due to the complexity of heavy oil, the intrinsic chemical reaction taking place in this partial upgrading process is generally explored by model systems. According to the available literatures, most of research mainly focuses on the hydrogenation of refractory heteroatoms-containing compounds [13–15], especially benzothiophene (BT) and 4, 6-dimethyldibenzothiophene (DBT).

Polyaromatic hydrocarbons (PAHs) are abundant in heavy oil. They are generally recognized as coke precursors during pyrolysis and environmental pollutants due to their toxicity and carcinogenicity [16–18]. A strict limitation for PAH content is the guarantee of the oil product quality [19]. Hence, hydrogenation of PAHs is essential for heavy oil efficient upgrading, as well as environmental protection [20]. Meanwhile, PAHs could act as effective hydrogen shuttle through generating hydroaromatics by partial hydrogenation. This is because hydroaromatics are well-known to be excellent hydrogen donors due to the relatively low C–H bond energy for naphthenic carbons in position β and α [21] (the bond energy data for alkanes, cycloalkanes, aromatics, and hydroaromatics with identical carbon numbers [22–25] are compared in Table S1 as supporting information). Utilization of PAHs as hydrogen shuttle/carriers could greatly improve the hydrogen assumption during heavy oil pyrolysis, which has been evidenced by previous researchers [26–29]. Therefore, a good knowledge of PAH partial hydrogenation with the low-cost and easily-accessible in situ hydrogen by WGSR to produce natural hydrogen donors is crucial to enhance hydrogen transferring behavior to postpone the coke formation and thus improve the upgrading efficiency of heavy oil [30–32].

In the present work, anthracene was selected as the model three-ring PAHs. Three different water-soluble and oil-soluble low-cost Fe-based compounds were used as catalysts. Hydrogenation of anthracene under CO-H_2O, N_2-H_2O and H_2-H_2O over these Fe-based catalysts was conducted. The comparative activity of in situ hydrogen from WGSR and molecular hydrogen for PAHs hydrogenation was studied. The exact catalytic fate of Fe-based catalysts was revealed by combining the thermogravimetric analysis (TG) as well as the X-ray diffraction (XRD), scanning electronic microscopy (SEM), and transmission electronic microscopy (TEM) of the decomposed species.

2. Results and Discussion

2.1. Partial Hydrogenation of Anthracene under CO-H_2O, N_2-H_2O, and H_2-H_2O over Fe-Based Catalysts

The anthracene hydrogenation experiments under CO-H_2O were firstly conducted over Fe-based catalysts at a temperature of 400 °C, an initial CO pressure of 2 MPa, and CO/H_2O molar ratio of 1/3. The conversion of CO and anthracene is shown in Figure 1. In the absence of catalysts, CO conversion is close to 7.5% after 120 min, and the anthracene conversion is lower than 10%. The amount of in situ hydrogen produced by WGSR and transferring to anthracene can be approximately calculated based on the conversion of CO and anthracene as well as their initial amounts. The detailed calculation process was given in Table S2 as supporting information. It can be estimated that after 120 min, about 0.085 mol of in situ hydrogen was produced while only 0.0053 mol of it transferred to anthracene. Based on the phase diagram, H_2O was in a gaseous state while anthracene was presented as the liquid phase under the experimental conditions. Hence, the anthracene hydrogenation could be restricted by the mass transfer between in situ hydrogen and anthracene as well as the limited hydrogen solubility due to the high diffusional resistance. It is the reason why supercritical water (SCW) has been introduced to promote the hydrogenation reactions by researchers [33,34]. The coke yield during bitumen upgrading

under SCW + CO is even lower than that under SCW + H_2, as stated by Sato et al. [35]. This is contrary to our previous report for residue upgrading at temperature of 400 °C and pressure lower than 10 MPa [12]. It can be inferred that the SCW facilitates the transferring of in situ hydrogen to heavy oil molecules. Nevertheless, the utilization of SCW with operating pressure higher than 22.1 MPa is partly constrained by the safety and high-cost problems. Upon the addition of Fe-based catalysts, both the WGSR and hydrogenation of anthracene to 9, 10-dihydroanthracene are promoted. The catalytic activity follows the order of $Fe(NO_3)_3{\cdot}9H_2O$ > FeNaph > $FeSO_4{\cdot}7H_2O$. It should be noted that the conversion of CO is not linearly correlated with the conversion of anthracene. The difference of catalytic activity for WGSR between FeNaph and $Fe(NO_3)_3{\cdot}9H_2O$ is apparently smaller than that for anthracene hydrogenation. This suggests that the sensitivity of WGSR and anthracene hydrogenation to Fe-based catalysts is different.

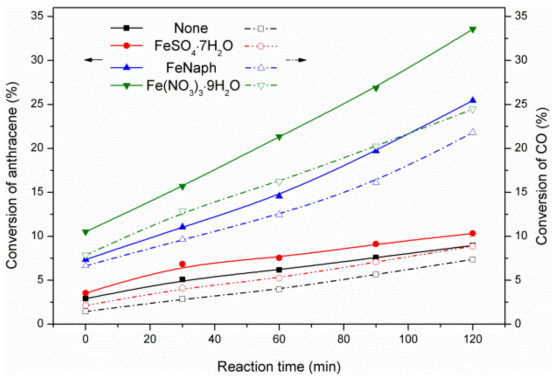

Figure 1. Reactant conversion during anthracene hydrogenation under CO-H_2O over different Fe-based catalysts.

Hydrogenation of anthracene under different atmospheres (i.e., N_2, H_2, and CO) and H_2O with or without $Fe(NO_3)_3{\cdot}9H_2O$ were carried out. A summary of the experimental runs is provided in Table 1, and the molar ratio of gas and water is 1:3. During experiment R3, the partial pressure of hydrogen is determined to be equivalent to the hydrogen amount generated by WGSR over Fe compounds under initial CO pressure of 2 MPa at reaction times of 0, 30, 60, 90 and 120 min (R4). The partial pressure of hydrogen in R1 and R2 corresponds to the maximum amount of hydrogen generated by WGSR in R4.

Table 1. A summary of the experimental runs.

Run. No.	Temperature/°C	Atmosphere (Initial Pressure/MPa)	Fe(NO3)3·9H2O/Fe wt%
R1	400	H2(0.50) + N2(1.50)	0.05
R2	400	H2(0.50) + N2(1.50)	0
R3	400	H2(x) + N2(2 − x)	0.05
R3(x = 0.16)	400	H2(0.16) + N2(1.84)	0.05
R3(x = 0.26)	400	H2(0.26) + N2(1.74)	0.05
R3(x = 0.32)	400	H2(0.32) + N2(1.68)	0.05
R3(x = 0.41)	400	H2(0.41) + N2(1.59)	0.05
R4	400	CO(2)	0.05
R5	400	CO(2)	0
R6	400	N2(2)	0
R7	400	N2(2)	0.05

Figure 2 presents the molar percentage of hydrogen in the gaseous products and the conversion of anthracene in these experimental runs. As the conversion of anthracene under N_2-H_2O is rarely detected in the case with or without $Fe(NO_3)_3{\cdot}9H_2O$ (R6 and R7), the introduction of water alone could not benefit the PAH hydrogenation and the Fe species have no influence on possible water activation to donate hydrogen. This is different from the aquathermolysis of heavy oil over Fe catalysts because

the key reaction during aquathermolysis is the cracking reaction of sulfur-containing compounds [36]. Under H_2-H_2O, the hydrogenation of anthracene is found to be a little promoted in the presence of $Fe(NO_3)_3{\cdot}9H_2O$ (R1 and R2), suggesting that the Fe species exhibit somewhat catalytic activity for activation of molecular hydrogen. It can be rationalized by the report that iron oxides (e.g., Fe_3O_4) could slightly catalyze the hydrogenation reactions during coal liquefaction [37,38]. Since the catalytic activity of iron oxides was reported to be lower than other sulfided species, molecular hydrogen displayed low hydrogenation activity. The formation of iron oxides is demonstrated in Section 3.3. In the case under CO-H_2O, both the amount of H_2 and anthracene conversion are remarkably increased by the addition of $Fe(NO_3)_3{\cdot}9H_2O$ (R4 and R5). On the whole, it can be concluded that the aid of Fe species for hydrogenation of anthracene under CO-H_2O is mainly attributed to its strong catalytic activity for the production of in situ hydrogen by WGSR.

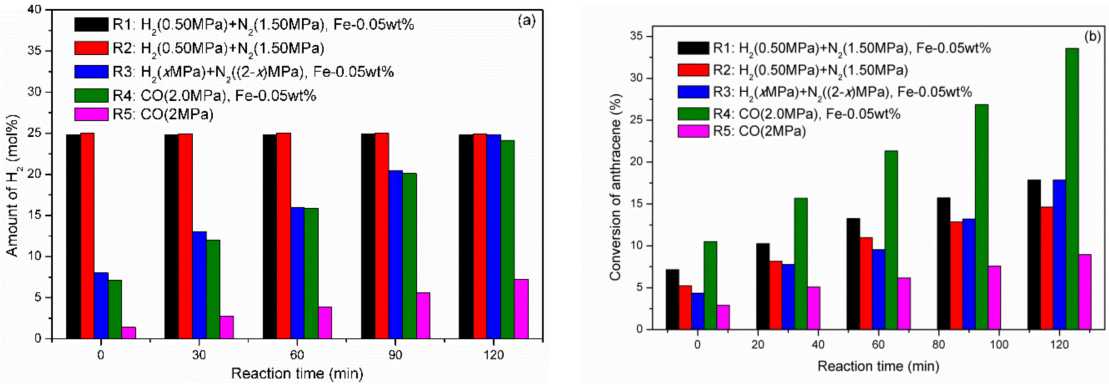

Figure 2. Comparison of anthracene hydrogenation in different experimental runs. (**a**) The amount of H_2; (**b**) the conversion of anthracene. In experiment R3, the *x* values for 0, 30, 60, 90, and 120 min are 0.16, 0.26, 0.32, 0.41, and 0.50, respectively.

2.2. Comparison of In Situ Hydrogen Produced by WGSR and Molecular Hydrogen

The comparison of in situ hydrogen produced by WGSR and molecular hydrogen remains a subject of debates in literatures. As aforementioned, in situ hydrogen presented higher activity for heavy oil partial upgrading over molecular hydrogen over dispersed catalysts [11]. And and Ng observed the same reactivity of in situ hydrogen as molecular hydrogen during hydrodesulfurization (HDS) of diesel fraction [39]. In the study of Takemura et al. [40], the in situ hydrogen was shown to be less active than molecular hydrogen for HDS of residual oil over supported Co-Mo/Al_2O_3 catalysts. Since the real oil system complicates the analysis, a part of researchers explored it by model compounds, especially sulfur-containing compounds. Ng et al. [8,9,13] and Liu et al. [41] reported that the reactivity of in situ hydrogen by WGSR was much higher than molecular hydrogen for hydrodesulfurization of DBT and BT using dispersed Mo catalysts. Hook et al. proposed that the in situ hydrogen was as effective as molecular hydrogen for HDS of DBT over supported Co-Mo/Al_2O_3 and Ni-Mo/Al_2O_3 catalysts [42]. Lee et al. ascribed the comparative activity of in situ hydrogen and molecular hydrogen to the ratio of H_2O to CO over dispersed Mo catalysts [43]. In the present work, it is believed that the mass transfer plays an important role in the hydrogenation of complex oil fractions. The further promotion of bitumen upgrading by SCW + CO than by SCW + H_2 could prove it, as studied by Sato et al. [35] and Jia [10]. Since these reported catalysts are efficient in both WGSR and hydrogenation, the in situ hydrogen produced by WGSR over the catalysts could be more possible to act on the target reactant than external supplied molecular hydrogen in terms of the mass transfer, leading to the relatively high reactivity of in situ hydrogen. On the other hand, the competitive adsorption of H_2O, CO, and CO_2 with reactant on the same active sites over the catalysts might result in the poor efficiency of hydrogenation with in situ hydrogen, as stated by Lee et al. [43]. Since the Fe-based catalysts herein have a single-function to catalyze WGSR, the competitive adsorption factor can be avoided, which facilitates the comparative study of the in situ hydrogen by WGSR and molecular hydrogen.

Although the same amount of hydrogen in R3 and R4 at different times is supplied, considerably higher anthracene conversion under CO-H_2O (R4) is achieved than using H_2-H_2O (R3). It is still the same result even for case R1 in which the amount of molecular hydrogen always keeps higher than the amount of in situ hydrogen produced from WGSR. Meanwhile, the hydrogenation rate also seems to be raised in the presence of in situ hydrogen. The correlation between anthracene conversion and the hydrogen amount is presented in Figure 3. Results show that the anthracene conversion seems to be linearly relevant to the amount of in situ hydrogen by WGSR instead of molecular hydrogen. This can be rationalized by the limited possibility of molecular hydrogen that could be dissolved in the liquids and then activated to form active hydrogen. Moreover, the phenomenon proves that the in situ hydrogen by WGSR is apparently more active than externally provided H_2. This corroborates well with the reports of Ng et al. [8,9,13]. If the contribution of molecular hydrogen for anthracene hydrogenation (R3) is deduced, the effective contribution of in situ hydrogen by WGSR in R4 could be as high as 15.7% at a time of 120 min.

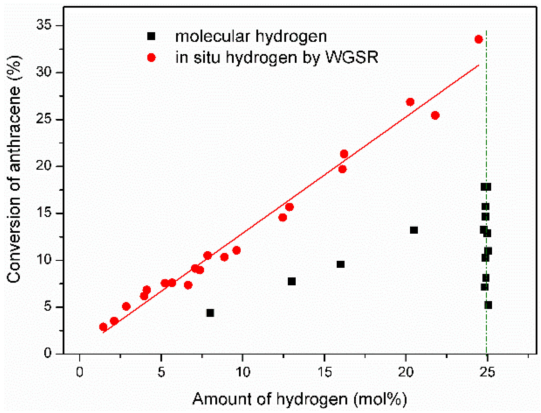

Figure 3. Correlation between anthracene conversion and hydrogen amount.

Additionally, Figure 4 displays the influence of anthracene hydrogenation on WGSR with or without Fe-based catalysts. It shows that the addition of anthracene increases the CO conversion, which can be attributed to the fact that WGSR is reversible. The hydrogen consumption by hydrogenation of anthracene could shift the equilibrium to the formation of hydrogen, thus promoting the CO conversion. The promotion result is further enhanced by the presence of Fe-based catalysts because of the higher hydrogen consumption. Hence, the synergism between WGSR and hydrogenation of anthracene exists. These results are well supported by the previous study of Ng et al. [13] that during HDS of benzothiophene with CO and H_2O, the rate constant of WGSR could be increased twice due to the addition of benzothiophene.

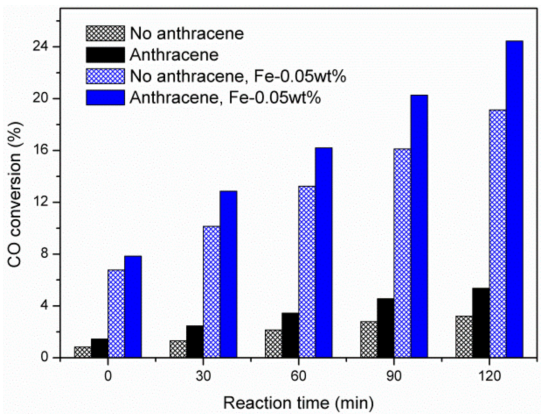

Figure 4. Effect of anthracene hydrogenation on CO conversion.

2.3. Characterization of Fe Catalytic Species during Hydrogenation of Anthracene under CO-H_2O

Section 2.1 shows that the Fe-based catalysts could promote the hydrogenation of anthracene under CO-H_2O due to their strong catalytic activity for WGSR and weak catalytic activity for hydrogenation. In order to reveal the exact component of catalytic species, the deposits from these iron precursors were characterized in detail. Figure 5 displays the weight loss curves (TG) and derivative weight loss curves (DTG) of FeNaph, $Fe(NO_3)_3{\cdot}9H_2O$, and $FeSO_4{\cdot}7H_2O$. Obviously, the whole decomposition of FeNaph could be mainly divided into two stages: (I) Temperature ranges from 25 to 336 °C with a mass loss of about 64.12%. The FeNaph sample is stored in solvent oil for stability and contains 5% Fe. The corresponding mass percentage of FeNaph and solvent oil in the sample is close to 35.55% and 64.45%, respectively. Hence, the mass loss in this stage could be assigned to the evaporation of solvent oil. (II) A mass loss of 28.72% from 335 to 551 °C, which is consistent with the mass loss of FeNaph to form Fe_2O_3. As for $FeSO_4{\cdot}7H_2O$, the seven H_2O molecules are lost in the temperature range of 25–275 °C with three stages. The final stage ranging from 481 to 656 °C with a mass loss of 25.09% represents the formation of Fe_2O_3. Concerning $Fe(NO_3)_3{\cdot}9H_2O$, two stages are observed in the TG and DTG plots. Based on the experimental mass loss, the first stage (25–126 °C) corresponds to the loss of nine H_2O molecules (32.44%). The temperature range from 150 to 350 °C with a mass loss of 42.52% is ascribed to the formation of Fe_2O_3. In view of the decomposition process, it can be inferred that $Fe(NO_3)_3{\cdot}9H_2O$ could be completely decomposed to Fe_2O_3 while FeNaph is only partly decomposed at the temperature of 400 °C. $FeSO_4{\cdot}7H_2O$ could just be subjected to the water loss stage, producing the $FeSO_4$ species.

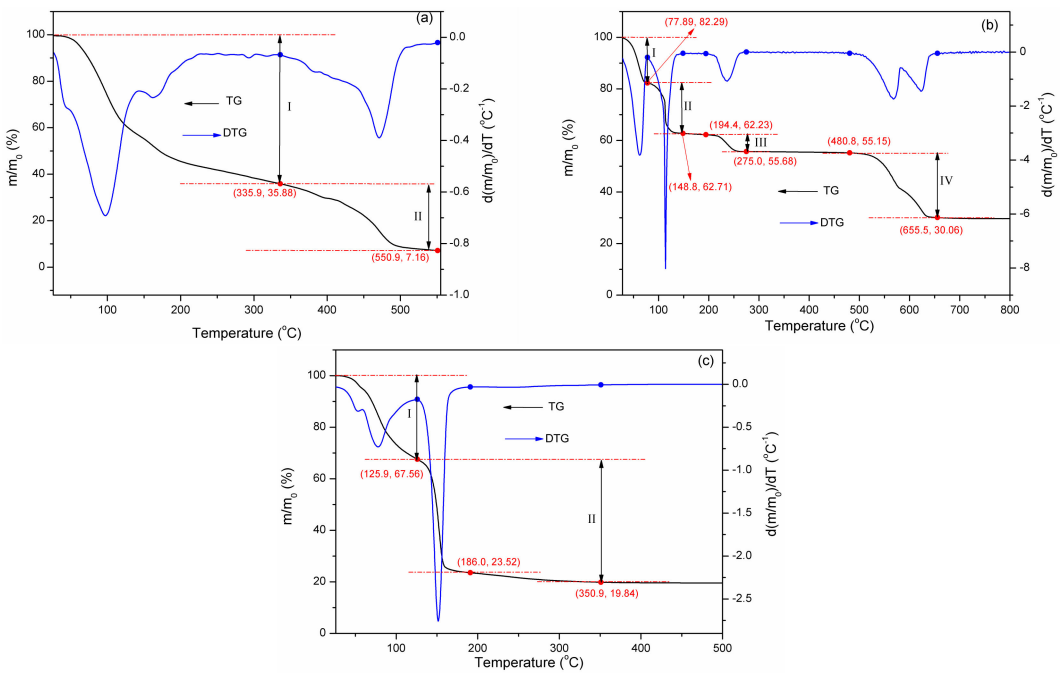

Figure 5. TG and DTG plots of different Fe-based catalysts. (**a**) FeNaph; (**b**) $FeSO_4{\cdot}7H_2O$; (**c**) $Fe(NO_3)_3{\cdot}9H_2O$.

Figure 6 shows the XRD patterns of the decomposition products of $Fe(NO_3)_3{\cdot}9H_2O$ under different atmospheres. The formation of Fe_2O_3 under N_2-H_2O evidenced from TG analysis is well supported by the characteristic XRD peaks at 2θ = 18.28°, 24.14°, 33.2°, 35.61°, 40.85°, 49.52°, 54.12°, 62.48°, and 71.96°. Additionally, they are shown as the α-Fe_2O_3 with hexagonal crystallographic structure. Under H_2-H_2O, the absorptions at 2θ = 18.60°, 30.08°, 35.44°, 37.08°, 43.09°, 56.96°, and 62.56° are observed in the XRD spectra of final Fe species. This clearly indicates the production of Fe_3O_4 with cubic crystallographic structure from the further reduction of Fe_2O_3 by hydrogen. Additionally, the typical peaks of Fe_2O_3 almost disappear in the XRD pattern of product obtained under H_2-H_2O.

It suggests that Fe_2O_3 could be completely reduced under the H_2 atmosphere. In the case of CO-H_2O, it can be obviously seen that both Fe_2O_3 from the decomposition of by $Fe(NO_3)_3{\cdot}9H_2O$ and Fe_3O_4 from further reduction of Fe_2O_3 by CO and H_2 have been generated. According to the research regarding WGSR catalysts, the Fe_3O_4 spinel is the active state responsible for the in situ hydrogen production from WGSR instead of Fe_2O_3 [44]. This explains the relatively high catalytic activity for hydrogenation of anthracene under CO and H_2O of FeNaph and $Fe(NO_3)_3{\cdot}9H_2O$.

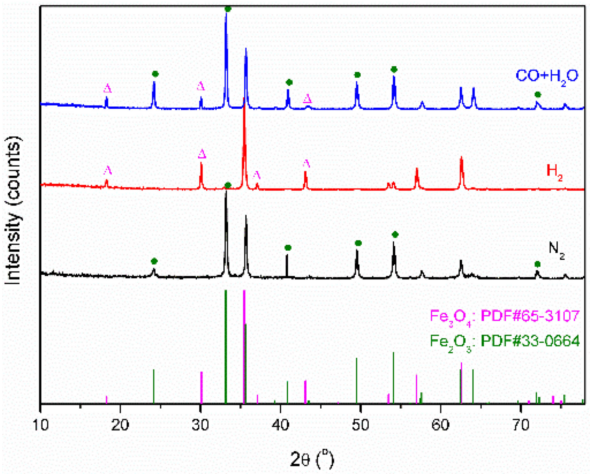

Figure 6. XRD patterns of decomposition products of $Fe(NO_3)_3{\cdot}9H_2O$ under different atmospheres. The green circle marks represent the characteristic peaks of Fe_2O_3, and the purple triangle marks represent the characteristic peaks of Fe_3O_4.

The species from the decomposition of $Fe(NO_3)_3{\cdot}9H_2O$ under CO and H_2O are further characterized by SEM and TEM, as shown in Figures 7 and 8, respectively. The SEM image clearly shows that the individual microsphere is composed of a large number of nanoparticles with a diameter ranging from 100 to 250 nm. These nanoparticles could be self-assembled to form a mesoporous network, which could favor the high surface area. The HRTEM image exhibits the lattice fringes with a spacing of about 0.37 nm that is characteristic of (012) basal planes of crystalline Fe_2O_3. Meanwhile, the fringes with a spacing of about 0.30 nm are also observed, which corresponds to the (220) basal planes of crystalline Fe_3O_4. This is further consistent with the XRD analysis result.

Since the in situ hydrogen displayed higher activity than molecular hydrogen, the possible forms of in situ hydrogen are then tentatively discussed. The associative mechanism and redox mechanism of WGSR have been widely-proposed [45], as compared in Figure 9. Both mechanisms have been supported by different experimental and theoretical analysis on various catalysts surface, including the Fe_3O_4 (111). It is recognized that the Fe_{tet1}- and $Fe_{oct2\text{-}tet1}$-terminated surfaces are the most stable terminations of the Fe_3O_4 (111) surface. As previously stated by Chen et al. [46], the $Fe_{oct2\text{-}tet1}$-terminated surface could be easily transformed into Fe_{tet1}-terminated surface under sufficient thermal treatment. Therefore, the Fe_{tet1}-terminated surface probably plays a key role in catalyzing the WGSR in the present work under 400 °C. The adsorption of H_2O on the Fe_3O_4 (111) surface is dominated by the Fe-O bond and the hydrogen bond between the surface O atom and an H atom in the H_2O molecule. Different from H_2O, CO is absorbed on the Fe_3O_4 (111) surface through the Fe-C bond by the back-donation of d-electron of Fe to the antibonding π *-orbital of CO. This suggests that H_2O and CO molecules could be activated when adsorbed on the catalysts. The TPD curves of H_2O and CO on the decomposed products displayed in Figure 10 could prove that the CO adsorption is superior to H_2O adsorption. When H_2O and CO co-adsorb on the Fe_3O_4 (111) surface, competition occurs, leading to the further elongation of Fe–O and Fe–C bonds. The activated H_2O is subsequently disassociated to the surface H * and OH * species. Even though the stronger adsorption tendency of CO than H_2O would inhibit this initial step for in situ hydrogen production, it is worth to be noted

that the higher amount of H_2O than CO with the molar ratio being 3 could facilitate the adsorption of H_2O in the present work.

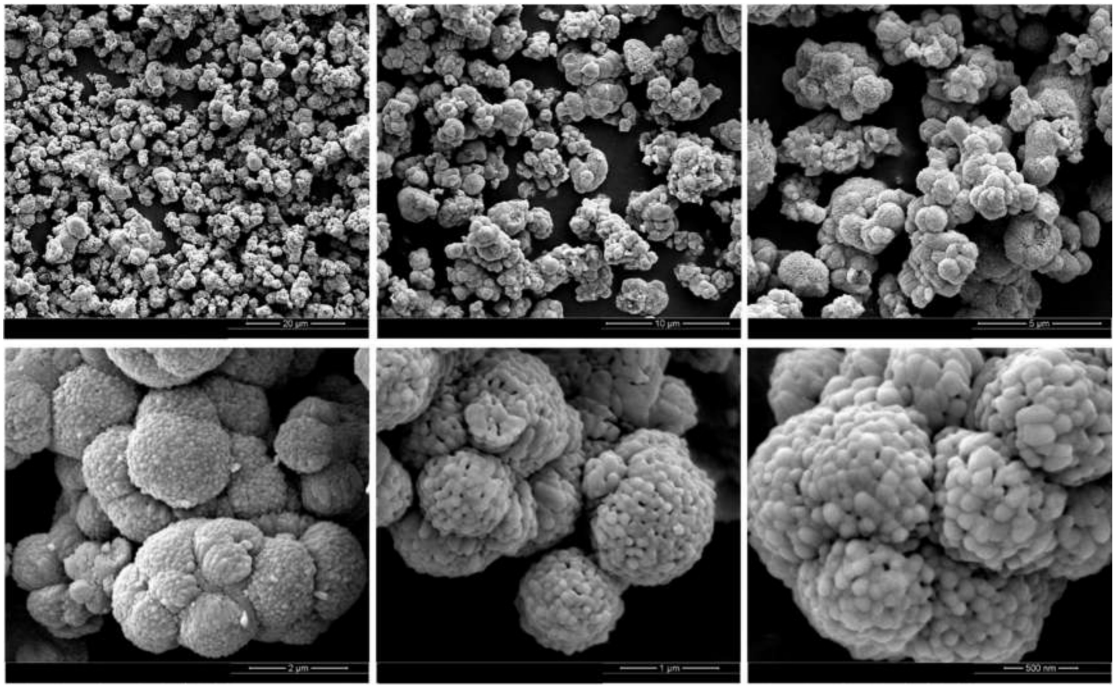

Figure 7. The SEM images of decomposition products of $Fe(NO_3)_3{\cdot}9H_2O$ under CO-H_2O.

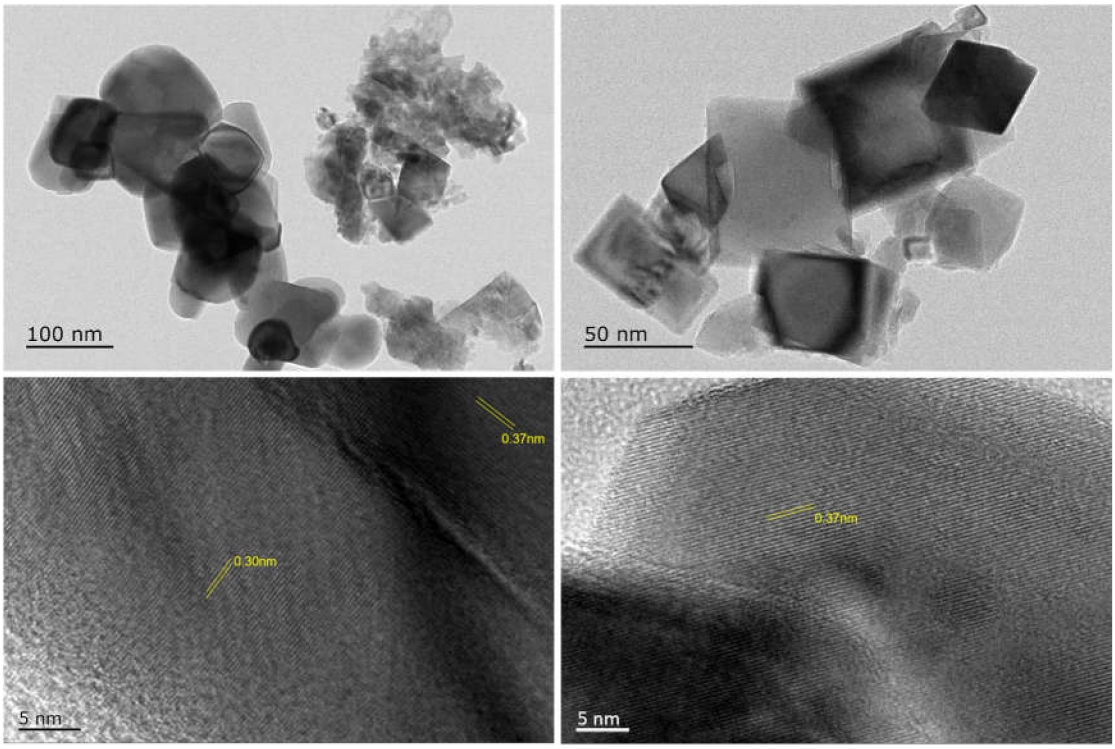

Figure 8. The high-resolution TEM images of decomposition products of $Fe(NO_3)_3{\cdot}9H_2O$ under CO-H_2O.

Redox mechanism	Associatvie mechanism
$H_2O* + * = HO* + H*$	$H_2O* + * = HO* + H*$
$HO* + * = H* + O*$	$HO* + *CO* = *COOH + *$
$*CO + O* = *CO_2 + *$	$*COOH + * = *CO_2 + H*$
$*CO_2 = CO_2 + *$	$*CO_2 = CO_2 + *$
$H* + H* = [H---H] + 2*$	$H* + H* = [H---H] + 2*$

Figure 9. The associative and redox mechanisms of WGSR on Fe_3O_4 (111) [45], * indicates an adsorption site.

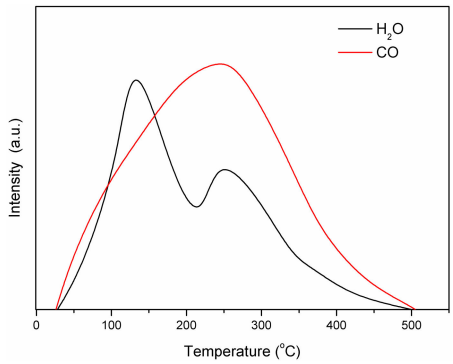

Figure 10. TPD curves of CO and H_2O on the decomposition products of $Fe(NO_3)_3{\cdot}9H_2O$ under CO-H_2O.

For the redox mechanism, the OH * species could then disassociate to form atomic H * and O *. In the presence of atomic O *, the CO molecule is oxidized to the surface COO * species. Meanwhile, the oxidation of CO is accomplished directly by OH * species to form a COOH * species as the intermediate for subsequent COO * formation during the associative mechanism. Finally, the surface COO * is desorbed to produce CO_2 and the two surface atomic H * are combined to produce H_2. Adschiri et al. ever found that CO_2 + H_2 + SCW and HCOOH + SCW were as efficient as CO + SCW for hydrogenation of hydrocarbons [47], implying the similarity of the reaction mechanism of producing in situ hydrogen. The theoretically calculated energy profiles reported by Chen et al. [46] suggested that the associative pathway for WGSR was preferred on Fe_{tet1}-terminated site of Fe_3O_4 (111) surface with the recombination of atomic H * being the rate-determining step. In this study under thermal conditions for heavy oil upgrading, it is reasonable to assume that the in situ hydrogen from WGSR catalyzed by Fe_3O_4 could stem from both the atomic H * and hydrogen in COOH * species. Furthermore, the hydrogen assumption by anthracene hydrogenation would promote the desorption of H * species and thus increase the WGSR conversion as shown by experimental results.

3. Materials and Methods

3.1. Materials

Anthracene (≥99.7%) was obtained from Aladdin Co., Ltd. (Shanghai, China), and toluene (≥99.7%) was purchased from Xilong Chemical Co., Ltd. (Shantou, Guangdong, China). $Fe(NO_3)_3{\cdot}9H_2O$ (≥99.7%) and $FeSO_4{\cdot}7H_2O$ (≥99.7%) were acquired from Sinopharm Chemical Reagent Co., Ltd. (Shanghai, China). FeNaph (≥99.7%, Fe: 5wt%) were bought from Xiya Chemical Co., Ltd. (Chengdu, Sichuan, China). All the chemicals were used without further purification.

3.2. Hydrogenation Experiment

All of the hydrogenation reactions were performed in a 500 mL CQF-0.5 batch autoclave produced from Dalian Jingyi autoclave limited company (Dalian, Liaoning, China) equipped with a sampling port. In a typical experiment, about 2.65 g of anthracene, 60 mL toluene, and a certain amount of

deionized water and Fe compounds were initially loaded into the autoclave. Toluene was selected as the solvent since anthracene is more soluble in toluene than other alkanes, and toluene is generally stable under the experimental condition. After purging with CO three times to remove as much air as possible, the autoclave was charged with a certain initial pressure of CO. Then it was stirred and heated to a given temperature. During the reaction progress, small amounts of liquid and gas sample were taken periodically. The liquid samples were immediately dissolved by toluene and centrifuged to remove the entrained water. When the reaction time was reached, the reactor was quenched with cool water to room temperature. The liquid samples were analyzed by gas chromatography (GC) using flame ionization detector (FID) (Bruker 450GC, Billerica, MA, USA) equipped with a capillary column (VF-1ms, 0.25 mm × 15 m × 0.25 μm). The gas samples were analyzed by GC using thermal conductivity detector (TCD) (Bruker 450GC, Billerica, MA, USA) with 5A molecular sieve column and Propark Q packed column. The composition was identified and quantified by using external standard model samples. The error analysis for typical experiments were shown in Figure S1 as supporting information. Additionally, the experimental error for conversion of CO and anthracene was within ± 3%.

3.3. Characterization of Catalytic Species

To understand the catalytic activity of Fe compounds, the TG analyses were performed on a Linseis STA PT1600 (Linseis Corporation, Selb, Bayern, Germany). The thermal decomposed products were collected and characterized by XRD, SEM and TEM. The XRD pattern was completed on an X'Pert PRO MPD diffractometer (PANalytical, Almelo, Netherland) with Cu Ka radiation at 40 kV and 40 mA. The SEM measurement was accomplished on a FEIQUANTAFEG250 scanning electron microscope (FEI company, Hillsboro, OR, USA). The TEM analysis was performed on an FEI Tecnai G2 F20 transmission electron microscope (FEI company, Hillsboro, OR, USA). The temperature programmed desorption (TPD) curves of CO and H_2O on the catalytic species were obtained using an Auto Chem 2920 Chemisorption apparatus (Micromeritics Instrument Corporation, Atlanta, GA, USA).

4. Conclusions

The Fe-based catalysts display obvious catalytic activity for anthracene hydrogenation under CO-H_2O instead of hydrogenation under N_2-H_2O and H_2-H_2O, and the activity follows in the order of $Fe(NO_3)_3{\cdot}9H_2O$ > Fe naphthenate > $FeSO_4{\cdot}7H_2O$. This suggests that they could significantly catalyze WGSR to produce in situ hydrogen. Even though the amount of molecular hydrogen remains higher than or equals to that of in situ hydrogen, the anthracene conversion with in situ hydrogen is remarkably higher. It demonstrates that the in situ hydrogen is more active than molecular hydrogen for PAHs hydrogenation. The exact fate of these Fe-based catalysts was explored by detailed characterization of decomposed products. It is found that Fe_2O_3 species could be formed by thermal treatment under N_2 and further reduced to Fe_3O_4 in the presence of H_2 and CO. It is the Fe_3O_4 species that play a key role in the hydrogenation of anthracene under CO and H_2O. The complete decomposition temperature for $Fe(NO_3)_3{\cdot}9H_2O$ is as low as 350 °C, consistent with its highest catalytic activity. Based on previous literatures, it is assumed that the in situ hydrogen could stem from the atomic H * and COOH * species adsorbed on the most possible Fe_{tet1}-terminated surface on $Fe_3O_4(111)$ at 400 °C. Given that heavy oil contains abundant polyaromatics, these results are meaningful for enhancing the hydrogen shuttling to heavy oil by in situ producing natural hydrogen donors, and thus benefiting the high-efficient upgrading.

Supplementary Materials: The following are available online at http://www.mdpi.com/2073-4344/10/12/1379/s1, Table S1. The typical C-H bond energy of different molecules. Table S2. Equations for the amount of in situ hydrogen calculation. Figure S1. The experimental error analysis for reactant conversion during typical anthracene hydrogenation under CO-H_2O over two Fe-based catalysts at a temperature of 400 °C, an initial CO pressure of 2 MPa and CO/H_2O molar ratio of 1/3. (a) Amount of H_2; (b) conversion of anthracene.

Author Contributions: Conceptualization, H.L., A.G. and Z.W.; methodology, H.L., S.F. and X.G.; software, H.L., S.F. and X.G.; validation, H.L., S.F. and J.W.; formal analysis, H.L., J.W. and K.C.; investigation, H.L. and Z.W.; resources, H.L. and A.G.; data curation, H.L. and S.F.; writing—original draft preparation, H.L.; writing—review and editing, J.W., K.C. and A.G.; visualization, A.G. and Z.W.; supervision, Z.W.; project administration, H.L. and Z.W.; funding acquisition, H.L. and Z.W. All authors have read and agreed to the published version of the manuscript.

Funding: This research was funded by the National Natural Science Foundation of China (21908248 and 21776313), the China Postdoctoral Science Foundation (2016M602219), the Provincial Natural Science Foundation of Shandong (ZR2017BB021), the Fundamental Research Funds for the Central Universities (19CX02013A), the Key Research and Development Plan of Shandong Province (2017GGX70108), and the China National Petroleum Corporation (PRIKY19022).

Acknowledgments: The authors are grateful to Bernard Wiafe Biney from Ghana for improving the English of this paper.

Conflicts of Interest: The authors declare no conflict of interest.

References

1. Borden, K. The challenges of processing and transporting heavy crude. *Oil Gas Facil.* **2015**, *2*, 22–26. [CrossRef]
2. Muñoz, J.A.D.; Ancheyta, J.; Castañeda, L.C. Required viscosity values to assure proper transportation of crude oil by pipeline. *Energy Fuels* **2016**, *30*, 8850–8854. [CrossRef]
3. Zhang, N.; Zhao, S.; Sun, X.; Xu, Z.; Xu, C. Storage stability of the visbreaking product from Venezuela heavy oil. *Energy Fuels* **2010**, *24*, 3970–3976. [CrossRef]
4. Wang, Q.; Wang, Z.; Zhuang, S.; Li, F.; Guo, L.; Guo, A. Thermal upgrading of inferior residue without or with hydrogen donor. *Acta Petrol. Sin. (Pet. Process. Sect.)* **2014**, *30*, 439–445.
5. Joshi, J.B.; Pandit, A.B.; Kataria, K.L.; Kulkarni, R.P.; Sawarkar, A.N.; Tandon, D.; Ram, Y.; Kumar, M.M. Petroleum residue upgradation via visbreaking: A review. *Ind. Eng. Chem. Res.* **2008**, *47*, 8960–8988. [CrossRef]
6. Gray, M.R.G.; Mccaffrey, W.C. Role of chain reactions and olefin formation in cracking, hydroconversion, and coking of petroleum and bitumen fractions. *Energy Fuels* **2002**, *16*, 756–766. [CrossRef]
7. Fischer, F.; Schrader, H. The production of oils by hydrogenation of coal. I. The hydrogenation of coal and other solid fuels by means of sodium formate. *Brennst. Chem.* **1921**, *2*, 161–173.
8. Ng, F.T.T.; Tsakiri, S.K. Activation of water in emulsion for catalytic desulphurization of benzothiophene. *Fuel* **1992**, *71*, 1309–1314. [CrossRef]
9. Ng, F.T.T. Upgrading heavy oil/bitumen emulsions via in situ hydrogen generation. *Prepr. Symp. Am. Chem. Soc. Div. Fuel Chem.* **1998**, *43*, 456–460.
10. Ng, F.T.T.; Moll, J. Hydrogen production from bitumen emulsion for desulfurization and upgrading. *Prepr. Symp. Am. Chem. Soc. Div. Fuel Chem.* **2012**, *57*, 853.
11. Jia, L. Oil Sands bitumen emulsion upgrading by using in situ hydrogen generated through the water gas shift reaction. Ph.D. Thesis, University of Waterloo, Waterloo, ON, Canada, December 2014.
12. Liu, H.; Wang, Z.; Zhao, X.; Li, Y.; Chen, K.; Guo, A. Partial upgrading of vacuum residue from Canadian oil sand bitumen under CO/H_2-H_2O. *J. Fuel Chem. Technol.* **2018**, *46*, 45–53.
13. Ng, F.T.T.; Milad, I.K. Catalytic desulphurization of benzothiophene in an emulsion via in situ generated H_2. *Appl. Catal. A* **2000**, *200*, 243–254. [CrossRef]
14. Liu, K. Hydrodesulfurization and hydrodenitrogenation of model compounds using in-situ hydrogen over nano-dispersed Mo sulfide based catalysts. Ph.D. Thesis, University of Waterloo, Waterloo, ON, Canada, October 2010.
15. Liu, K.; Ng, F.T.T. Effect of the nitrogen heterocyclic compounds on hydrodesulfurization using in situ hydrogen and a dispersed Mo catalyst. *Catal. Today* **2010**, *149*, 28–34. [CrossRef]
16. Yue, X.M.; Wei, X.Y.; Zhang, S.Q.; Liu, F.J.; Zong, Z.M.; Yang, X.Q. Hydrogenation of polycyclic aromatic hydrocarbons over a solid superacid. *Fuel Process. Technol.* **2017**, *161*, 283–288. [CrossRef]
17. Schachtl, E.; Zhong, L.; Kondratieva, E.; Hein, J.; Gutiérrez, O.Y.; Jentys, A.; Lercher, J.A. Understanding Ni promotion of MoS_2/γ-Al_2O_3 and its implications for the hydrogenation of phenanthrene. *ChemCatChem* **2016**, *7*, 4118–4130. [CrossRef]

18. Fan, H.; Wu, T.; Yang, G.; Zhang, P.; Ding, G.; Wang, W.; Jiang, T.; Han, B. Effect of CO_2/water mixture on the selective hydrocracking of anthracene. *Catal. Commun.* **2013**, *33*, 42–46. [CrossRef]
19. Cai, X.; Long, J.; Wang, N.; Zhu, X.; Liu, Z.; Liu, Y.; Tian, S. Molecular characterization and transformation of PAHs in the hydrotreating process of light cycle oil. *Acta Petrol. Sin. (Pet. Process. Sect.)* **2017**, *33*, 403–410.
20. Liu, H.; Ji, S.; Wang, Z.; Guo, A.; Chen, K. The catalytic performance of metalloporphyrins during hydrogenation of anthracene. *Energy Technol.* **2015**, *3*, 145–154. [CrossRef]
21. Alemán-Vázquez, L.O.; Torres-Mancera, P.; Ancheyta, J.; Ramírez-Salgado, J. Use of hydrogen donors for partial upgrading of heavy petroleum. *Energy Fuels* **2016**, *30*, 9050–9060. [CrossRef]
22. Yang, Z.; Zong, S.; Long, J. Quantum mechanical studies on the micro-structure of tetrahydro-naphthalene. *Comput. Appl. Chem.* **2012**, *29*, 465–468.
23. Ye, W. The primary exploration on the chemical structure and refining properties of different types of petroleum molecules. Ph.D. Thesis, Research Institute of Petroleum Processing, Beijing, China, June, 2016.
24. Luo, Y. *Handbook of Chemical Bond Energies*; Science Press: Beijing, China, 2005.
25. Jiang, X.; Zong, S.; Li, X.; Zhao, Y. Molecular simulation of the hydrogen donating ability of hydrocarbon molecule. *Acta Petrol. Sin. (Pet. Process. Sect.)* **2012**, *28*, 254–259.
26. Alemán-Vázquez, L.O.; Cano-Domínguez, J.L.; García-Gutiérrez, J.L. Effect of tetralin, decalin and naphthalene as hydrogen donors in the upgrading of heavy oils. *Procedia Eng.* **2012**, *42*, 532–539. [CrossRef]
27. Kim, S.H.; Kim, K.D.; Lee, H.; Lee, Y.K. Beneficial roles of H-donors as diluent and H-shuttle for asphaltenes in catalytic upgrading of vacuum residue. *Chem. Eng. J.* **2017**, *314*, 1–10. [CrossRef]
28. Kubo, J.; Higashi, H.; Yoshiharu Ohmoto, A.; Arao, H. Heavy oil hydroprocessing with the addition of hydrogen-donating hydrocarbons derived from petroleum. *Energy Fuels* **1996**, *10*, 474–481. [CrossRef]
29. Wang, Z.; Ji, S.; Liu, H.; Chen, K.; Guo, A. Hydrogen transfer of petroleum residue subfractions during thermal processing under hydrogen. *Energy Technol.* **2015**, *3*, 259–264. [CrossRef]
30. Guo, A.; Wang, Z.; Zhang, H.; Zhang, X.; Wang, Z. Hydrogen transfer and coking propensity of petroleum residues under thermal processing. *Energy Fuels* **2010**, *24*, 3093–3100. [CrossRef]
31. Sheng, Q.; Wang, G.; Duan, M.; Ren, A.; Yao, L.; Hu, M.; Gao, J. Determination of hydrogen-donating ability of industrial distillate narrow fractions. *Energy Fuels* **2016**, *30*, 10314–10321. [CrossRef]
32. Gould, K.A.; Wiehe, I.A. Natural hydrogen donors in petroleum resids. *Energy Fuels* **2007**, *21*, 1199–1204. [CrossRef]
33. Li, N.; Yan, B.; Xiao, X. A review of laboratory-scale research on upgrading heavy oil in supercritical water. *Energies* **2015**, *8*, 8962–8989. [CrossRef]
34. Arai, K.; Tadafumi Adschiri, A.; Watanabe, M. Hydrogenation of hydrocarbons through partial oxidation in supercritical water. *Ind. Eng. Chem. Res.* **2010**, *7*, 273–281. [CrossRef]
35. Sato, T.; Sumita, T.; Itoh, N. Effect of CO addition on upgrading bitumen in supercritical water. *J. Supercrit. Fluids* **2015**, *104*, 171–176. [CrossRef]
36. Maity, S.K.; Ancheyta, J.; Marroquín, G. Catalytic aquathermolysis used for viscosity reduction of heavy crude oils: A review. *Energy Fuels* **2010**, *24*, 2809–2816. [CrossRef]
37. Li, Y.; Cao, Y.; Jia, D. Direct coal liquefaction with Fe_3O_4 nanocatalysts prepared by a simple solid-state method. *Energies* **2017**, *10*, 886. [CrossRef]
38. Weng, S.; Gao, J.; Wu, Y.; Zhao, C.; Wu, Z. Mossbauer spectroscopic study of iron catalyst in coal hydroliquefaction II. On the transformation and the hydrogenation activity of ferric oxide under various reaction conditions. *J. Fuel Chem. Technol.* **1990**, *18*, 103–108.
39. Siewe, C.N.S.; Ng, F.T.T. Hydrodesulfurization of cold lake diesel fraction using dispersed catalysts: Influence of hydroprocessing medium and sources of H_2. *Energy Fuels* **1998**, *12*, 598–606. [CrossRef]
40. Takemura, Y.; Itoh, H.; Ouchi, K. Catalytic hydrodesulfurization of residual oil by a mixture of carbon monoxide and water. *Sekiyu Gakkaishi* **2008**, *24*, 357–362. [CrossRef]
41. Liu, C.; Ng, F.T.T. HDS of DBT using in situ generated hydrogen in the presence of dispersed Mo catalysts II. Comparison between in situ hydrogen and molecular H_2. *Chin. J. Catal.* **1999**, *20*, 505–510.
42. Hook, B.D.; Akgerman, A. Desulfurization of dibenzothiophene by in-situ hydrogen generation through a water gas shift reaction. *Ind. Eng. Chem. Process Des. Dev.* **1986**, *25*, 278–284. [CrossRef]
43. Lee, R.Z.; Ng, F.T.T. Effect of water on HDS of DBT over a dispersed Mo catalyst using in situ generated hydrogen. *Catal. Today* **2006**, *116*, 505–511. [CrossRef]

44. Patlolla, A.; Carino, E.V.; Ehrlich, S.N.; Stavitski, E.; Frenkel, A.I. Application of operando XAS, XRD, and Raman spectroscopy for phase speciation in water gas shift reaction catalysts. *ACS Catal.* **2013**, *2*, 2216–2223. [CrossRef]
45. Huang, L.; Han, B.; Zhang, Q.; Fan, M.; Cheng, H. Mechanistic study on water gas shift reaction on the Fe_3O_4 (111) reconstructed surface. *J. Phys. Chem. C* **2015**, *119*, 28934–28945. [CrossRef]
46. Chen, L.; Ni, G.; Han, B.; Zhou, C.; Wu, J. Mechanism of water gas shift reaction on Fe_3O_4 (111) surface. *Acta Chim. Sin.* **2011**, *69*, 393–398.
47. Adschiri, T.; Shibata, R.; Sato, T.; Masaru Watanabe, A.; Arai, K. Catalytic hydrodesulfurization of dibenzothiophene through partial oxidation and a water-gas shift reaction in supercritical water. *Ind. Eng. Chem. Res.* **1998**, *37*, 2634–2638. [CrossRef]

Publisher's Note: MDPI stays neutral with regard to jurisdictional claims in published maps and institutional affiliations.

© 2020 by the authors. Licensee MDPI, Basel, Switzerland. This article is an open access article distributed under the terms and conditions of the Creative Commons Attribution (CC BY) license (http://creativecommons.org/licenses/by/4.0/).